Magnesium thermal reduction of phytolith for high-performance three dimensional hierarchical C/Si@Si nanoparticle@reduced graphene oxide composite anode

Pengbo Xiao[a], Xiaocheng Li[a,c,*], Wenhui Xie[a], Wenhao Chen[a], Peng Huang[b*], Tengyun Zuo[b], Qing Zhang[b], Xi Liu[b], Sydorov Dmytro[a]

[a]*Jiangxi Provincial Key Laboratory of Power Batteries & Energy Storage Materials, Faculty of Materials Metallurgy and Chemistry, Jiangxi University of Science and Technology, Ganzhou Jiangxi 341000, P.R. China*

[b]*Natural Resources Rights and Reserves Security Centre, Jiangxi Provincial Natural Resources Department, Nanchang, Jiangxi, 330025, P.R. China*

[c]*Yichun Lithium New Energy Industry Research Institute, Jiangxi University of Science and Technology, Yichun 360904 P.R. China*

Email: xiaocheng_li@jxust.edu.cn; 87210760@qq.com

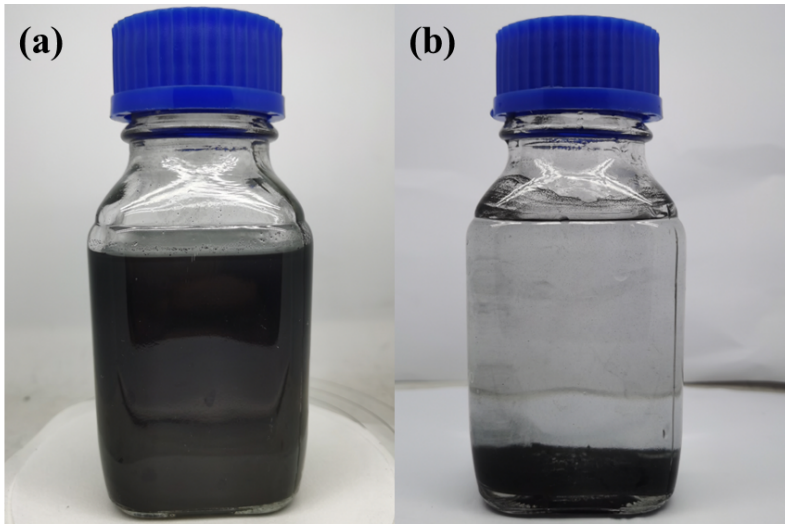

Fig. S1 (a,b) The upper aqueous solution clarifies before and after.

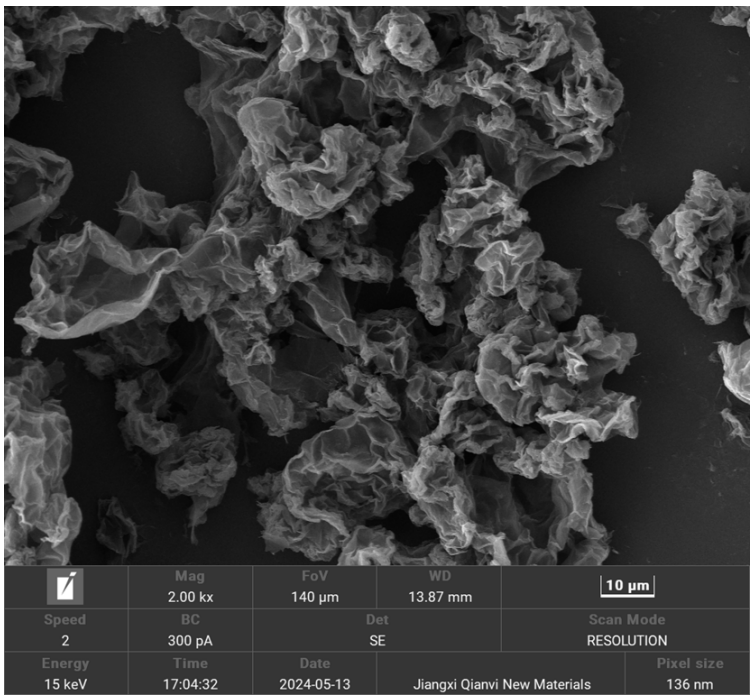

Fig. S2 SEM image of the GO.

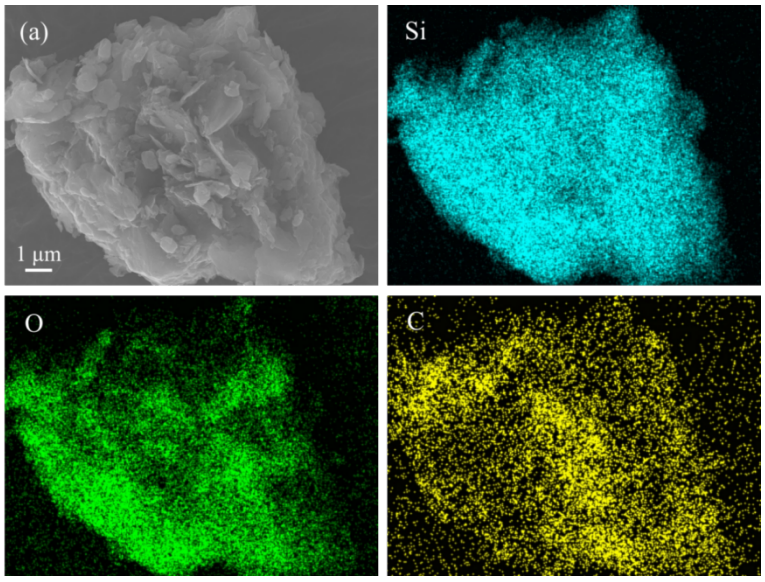

Fig. S3 SEM images of pristine phytolith and EDS mapping spectra of the pristine phytolith.

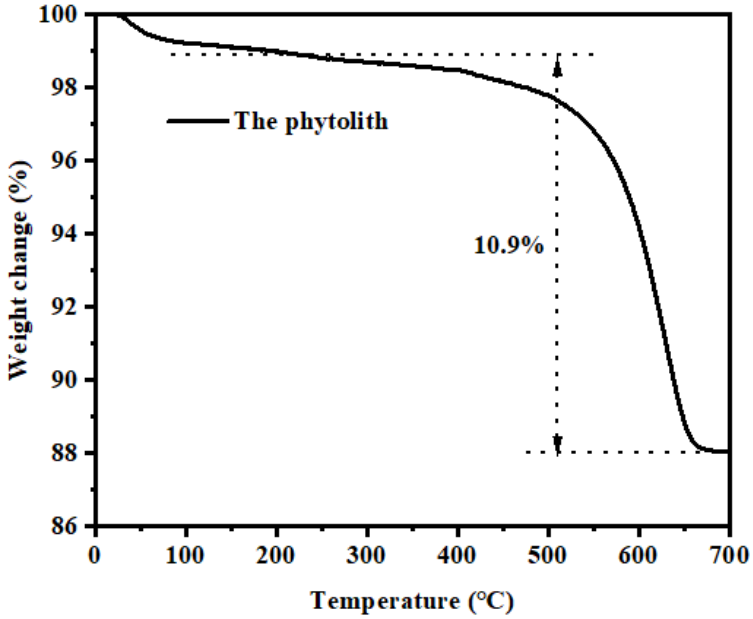

Fig. S4 TGA curves of the pristine phytolith.

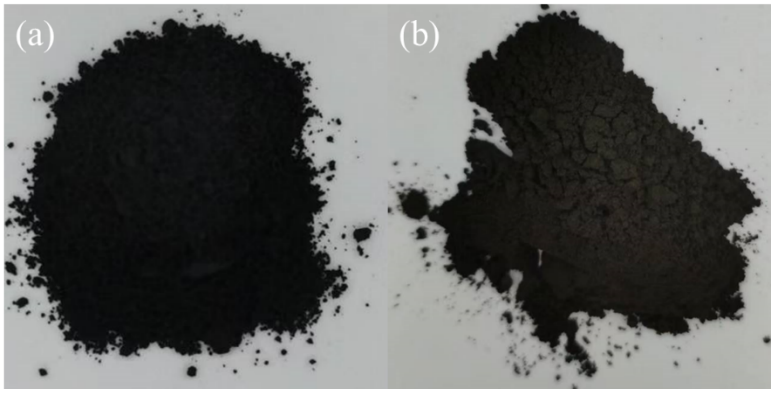

Fig. S5 The digital images of (a) etched layered phytolith and (b) the reduced phytolith.

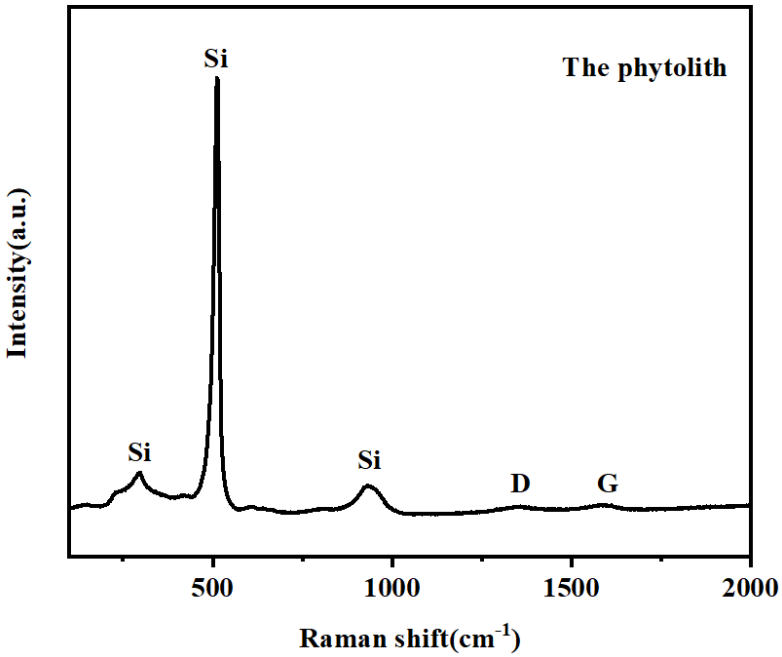

Fig. S6 Raman spectrum of the reduced phytolith.

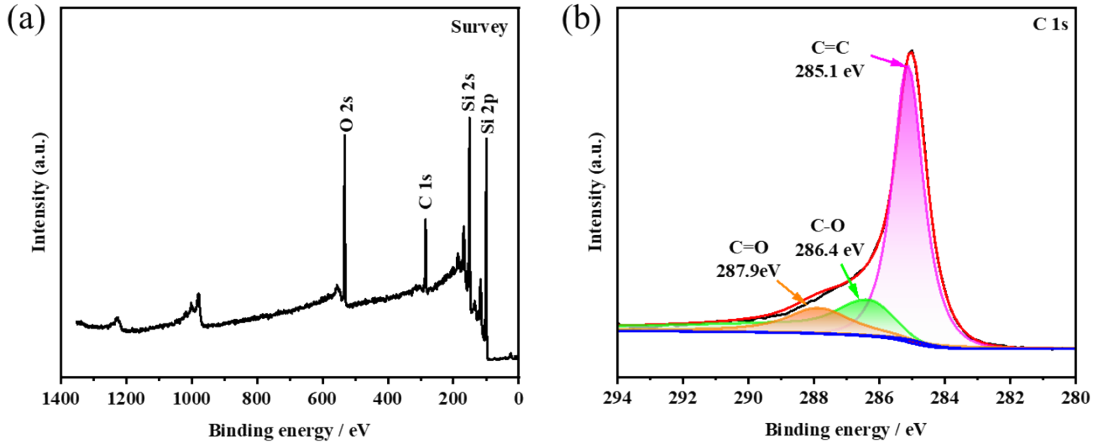

Fig. S7 (a) Survey spectra and (b) High-resolution XPS C 1s spectrum of the C/Si@SiNPs.

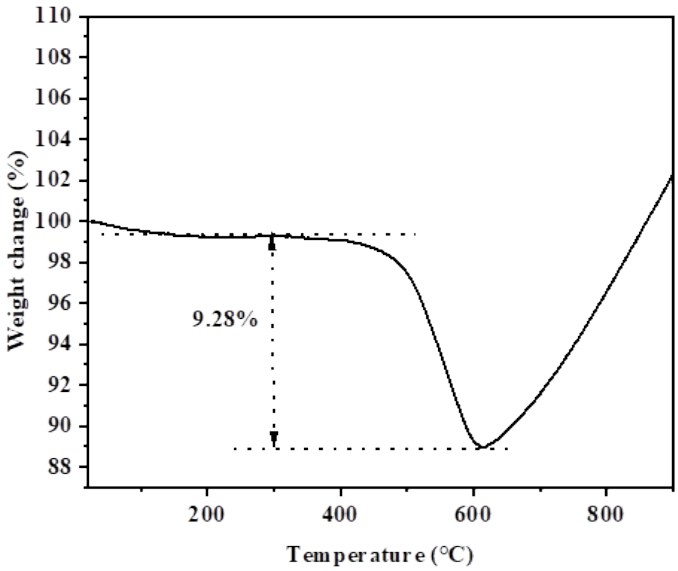

Fig. S8 TGA curves of the C/Si@SiNPs

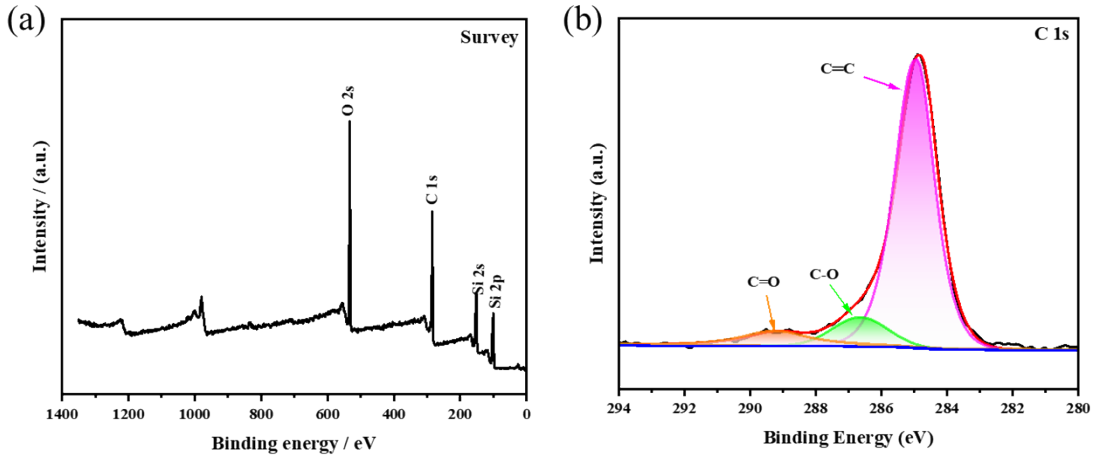

Fig. S9 (a) Survey spectra and (b) High-resolution XPS C 1s spectrum of C@SiNPs@rGO.

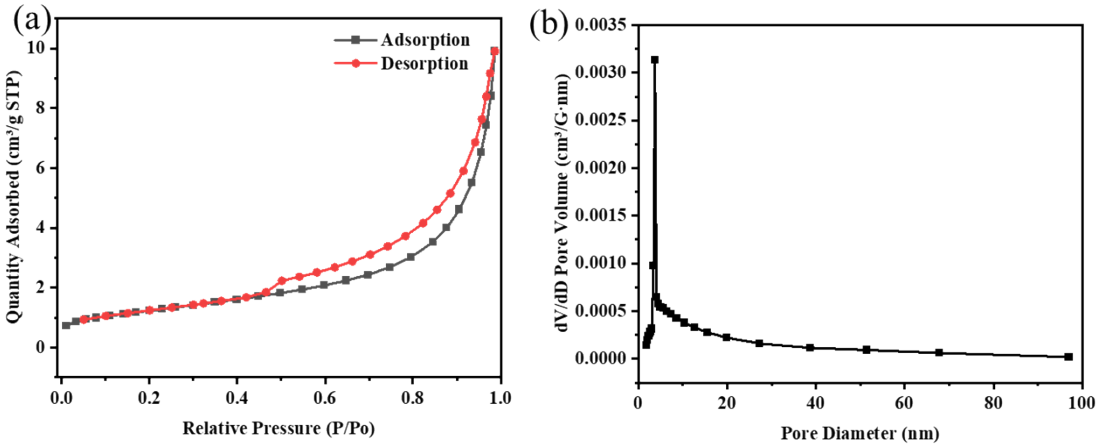

Fig. S10 (a) N_2 adsorption–desorption isotherms and(b) Pore size distributions of the etched phytolith.

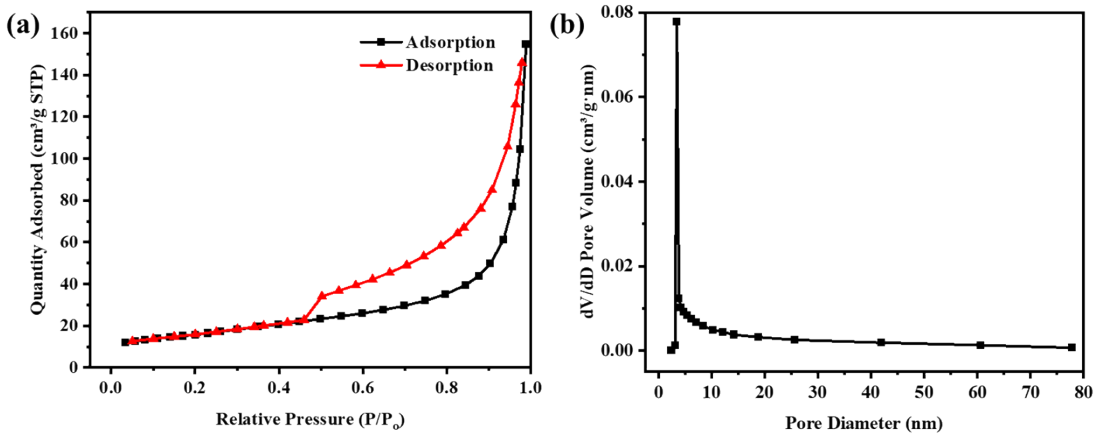

Fig. S11 (a) N_2 adsorption–desorption isotherms and(b) Pore size distributions of the rGO.

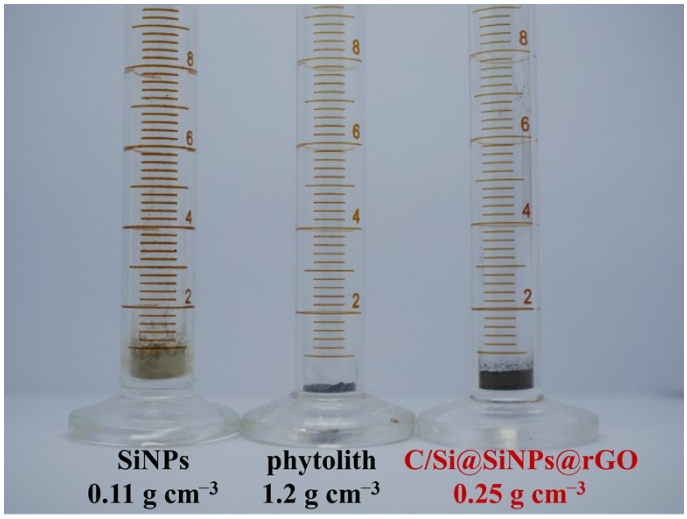

Fig. S12 The digital images of the same amount (100 mg) of the commercial SiNPs, phytolith and C/Si@SiNPs@rGO. The tap densities of the commercial SiNPs, C/Si@SiNPs and C/Si@SiNPs@rGO exhibit 0.11 g cm^{-3}, 1.2 g cm^{-3} and 0.25 g cm^{-3}, respectively.

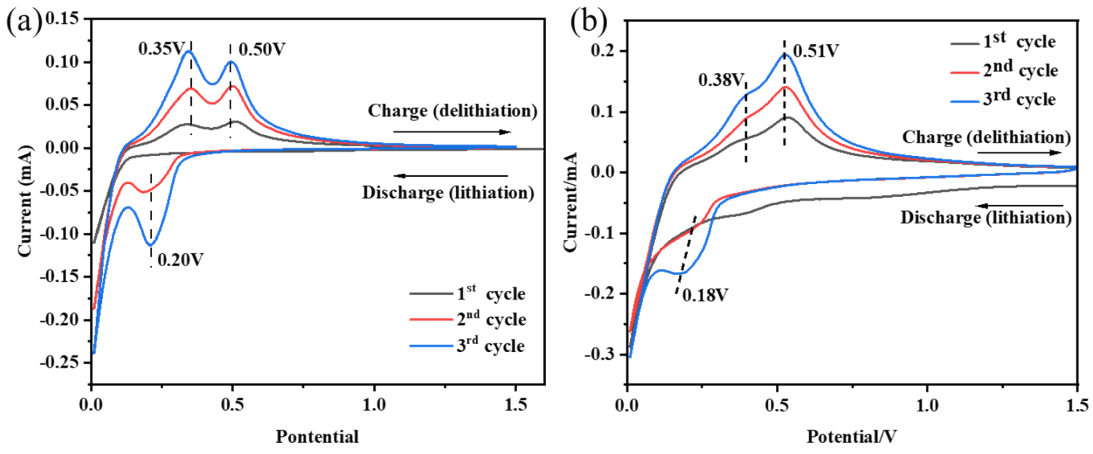

Fig. S13 (a, b) CV curves of the nom-Si and C/Si@SiNPs@rGO anodes.